

Higgs-mediated optical amplification in a non-equilibrium superconductor

Michele Buzzi,¹ Gregor Jotzu,¹ Andrea Cavalleri,¹ J. Ignacio Cirac,² Eugene A. Demler,³ Bertrand I. Halperin,³ Mikhail D. Lukin,³ Tao Shi,⁴ Yao Wang,³ and Daniel Podolsky^{*5}

¹*Max Planck Institute for the Structure and Dynamics of Matter, 22761 Hamburg, Germany*

²*Max Planck Institute for Quantum Optics, 85748 Garching, Germany*

³*Department of Physics, Harvard University, Cambridge, MA 02138, USA*

⁴*CAS Key Laboratory of Theoretical Physics, Institute of Theoretical Physics, Chinese Academy of Sciences, Beijing 100190, China*

⁵*Physics Department, Technion, 32000 Haifa, Israel*

The quest for new functionalities in quantum materials has recently been extended to non-equilibrium states, which are interesting both because they exhibit new physical phenomena and because of their potential for high-speed device applications. Notable advances have been made in the creation of metastable phases^{1–9} and in Floquet engineering under external periodic driving^{10–12}. In the context of non-equilibrium superconductivity, examples have included the generation of transient superconductivity above the thermodynamic transition temperature^{6–8,13,14}, the excitation of coherent Higgs mode oscillations^{15–18} and the optical control of the interlayer phase in cuprates^{19,20}. Here, we propose theoretically a novel non-equilibrium phenomenon, through which a prompt quench from a metal to a transient superconducting state could induce large oscillations of the order parameter amplitude. We argue that this oscillating mode could act as a source of parametric amplification of the incident radiation. We report experimental results on optically driven K_3C_{60} that are consistent with these predictions. The effect is found to disappear when the onset of the excitation becomes slower than the Higgs mode period, consistent with the theory proposed here. These results open new possibilities for the use of collective modes in many-body systems to induce non-linear optical effects.

I. INTRODUCTION

The Higgs mode is a fundamental collective excitation of systems with spontaneous symmetry breaking. It is a gapped excitation associated with oscillations of the amplitude of the order parameter. Examples of the Higgs mode in condensed matter are plentiful: it has been observed in the superconducting phase of $NbSe_2$ ^{21–23} and of amorphous superconducting films²⁴, in the dimerized antiferromagnet $TlCuCl_3$ ²⁵, in a variety of incommensurate charge density wave (CDW) systems^{26–28}, and in cold bosonic gases near the superfluid to Mott insulator transition^{29,30}.

In a number of experiments reported recently, superconductivity is created non-adiabatically after a rapid change in microscopic interactions, as induced by the application of a terahertz or mid-infrared (MIR) pump pulse^{31–34}. Although the dynamics of this process are not yet fully understood, we posit that the “Mexican hat” effective potential for the superconducting order parameter is established promptly after optical excitation, see Fig. 1(a). The appearance of large Higgs oscillations is then a natural attribute of such photo-induced superconductivity if the quench is fast compared to the frequency of the Higgs mode ω_H , see Fig. 1(b) (the order parameter dynamics following a sudden quantum quench has been studied theoretically in a number of related contexts, see, *e.g.*, Refs. 35–38).

We argue that in this situation, the coherent collective mode can act as a source of parametric amplification³⁹ for oscillations of long-lived phase fluctuations resulting in an enhanced reflectivity for a time-delayed probe pulse. This phenomenon can be qualitatively understood as a superconductor with an excited Higgs mode, which then places a parametric modulation on low-frequency phase modes. We predict that the reflected beam would then feature amplification of intensity at the original frequency ω_1 , as well as the generation of an idler signal at the complementary frequency $\omega_H - \omega_1$ (see Fig. 1(c)). We dub this phenomenon “Higgs amplification”.

We also report experimental results on optically driven K_3C_{60} , which support these predictions. Using a pump-probe technique, we illuminate our samples with a pump pulse at 41 THz, and a probe pulse spanning frequencies between 1 to 7 THz. Phase-resolved detection of the reflected signal allows us to reconstruct both the real and imaginary parts of the conductivity at the probe frequency. We find that when K_3C_{60} is driven with pump pulses of suitable duration, the incident probe light is locally amplified near the surface for frequencies below 10 meV/ \hbar . We analyze experimental results taking into account penetration depth mismatch between the pump and probe pulses. We observe an anomalous enhancement of the reflectance, which in an homogeneously excited medium would result in 6% amplification. For the penetration depth of the probe beam of 700 nm this corresponds to the amplification coefficient $\alpha \sim 10^3$ cm⁻¹.

Our underlying theoretical considerations are presented in Sections II and III, below. Experimental results are presented in Section IV, and a comparison of theory

*Corresponding author: podolsky@physics.technion.ac.il

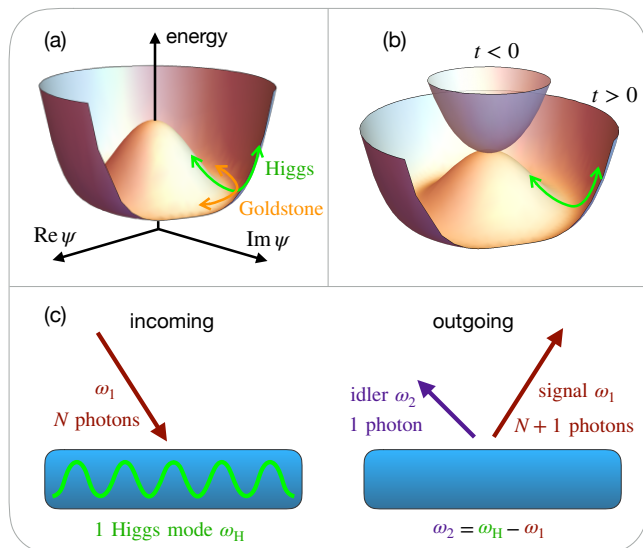


FIG. 1: (a) Schematic potential in a broken symmetry state. The collective excitations are Goldstone and Higgs modes. (b) A sudden change in system parameters at time $t = 0$ leads to a rapid inversion in the potential, thus inducing Higgs oscillations. (c) Light amplification in a superconductor with an excited Higgs mode. Left panel: A probe pulse containing N photons of frequency ω_1 is incident on a superconductor with an excited Higgs mode (represented by a wave). Right panel: The output consists of $N + 1$ photons of frequency ω_1 , plus a single photon of frequency ω_2 traveling “backward”, due to in-plane momentum conservation. When many Higgs excitations undergo stimulated decay, a large number of both ω_1 and ω_2 photons are produced.

and experiment is given in Section V. Some implications of this work, and the outlook for further developments, are given in Section VI. Additional details of our analysis are given in three appendices.

II. FROM HIGGS OSCILLATIONS TO ANOMALOUS REFLECTION

The coupling between the Higgs mode and light can be understood by observing that in a general state with broken continuous symmetry, the Higgs mode can decay into a pair of Goldstone modes. For neutral superfluids, this process determines the lifetime of Higgs excitations⁴⁰. In superconductors, the Goldstone mode describes phase fluctuations and therefore a charge current, which interacts directly with photons. Deep inside the material, these photons are gapped to the plasma frequency by the Anderson-Higgs mechanism, thus protecting the Higgs mode from decay. However, near the surface, a Higgs excitation can decay into a pair of gapless vacuum photons whose frequencies add up to ω_H .

This corresponds to an effective term in the Hamiltonian

$$\mathcal{H}_{\text{Higgs/photons}} \sim \sum_{\omega_1 + \omega_2 = \omega_H} (h a_{\omega_1}^\dagger a_{\omega_2}^\dagger + h^\dagger a_{\omega_1} a_{\omega_2}) \quad (1)$$

where h is a quantum field that annihilates a Higgs excitation and a_ω annihilates a vacuum photon of frequency ω . Hence, the energy of the excited Higgs mode is converted into entangled photon pairs. In the absence of the probe pulse, all photon pairs are generated equally. However, the incoming probe enhances the generation of pairs in which one of the photons matches the incident photons because of the bosonic stimulation factor.

One can understand the origin of the coupling in Eq. (1) from the following consideration. In superconductors, the diamagnetic coupling term between light and matter, $H_{\text{dia}} = \frac{e^2 \hbar^2}{2m c^2} n_s \mathbf{A}^2$, plays a key role, giving rise to the London equation for the current response to an electromagnetic field and to the Meissner effect. Here, n_s is the superfluid density which, for a coherently excited Higgs mode, is expected to oscillate at the Higgs frequency, $n_s = n_{s,0} + \delta n \cos(\omega_H t)$. In a quantized description of the electromagnetic field, the vector potential \mathbf{A} is a linear combination of photon creation and annihilation operators, schematically of the form $\mathbf{A} \sim \sum_{\omega} (a_{\omega} + a_{\omega}^\dagger)$. This implies that the diamagnetic term gives rise to the term (1), where h is a quantum analog of the oscillating part of the superfluid density δn . Interactions of this type are known to give rise to stimulated emission and parametric down conversion of light⁴¹.

These considerations give rise to the following mechanism of Higgs amplification. Consider an incident probe pulse composed of N photons at frequency $\omega_1 < \omega_H$ as it is reflected from a superconductor. The term $a_{\omega_1}^\dagger a_{\omega_2}^\dagger$ creates a pair of photons, leading to a state with $N + 1$ photons at ω_1 and one $\omega_2 = \omega_H - \omega_1$ photon, see Fig. 1(c). The amplitude of this process is enhanced by a Bose factor of $\sqrt{N + 1}$. As long as the Higgs mode remains excited, this process leads to amplification of ω_1 photons and generation of ω_2 photons, until the Higgs mode is depleted. The net effect is outgoing light with two frequencies, ω_1 and ω_2 , related by $\omega_1 + \omega_2 = \omega_H$, and the outgoing light at ω_1 having a higher intensity than the incoming signal.

In typical superconductors, the Higgs frequency is smaller than the plasma frequency. Then, incident light with $\omega_1 < \omega_H$ does not penetrate deeply into the material, and Higgs amplification is a surface effect. In particular, due to the evanescent nature of the waves inside the material, there are no phase matching conditions in this process. This means that there isn't a discrete set of frequencies at which Higgs amplification is resonantly enhanced, and hence the level of amplification is expected to depend smoothly on the probe frequency ω_1 . The frequency scale for the Higgs mode is comparable to the superconducting gap. Hence, for many superconductors, Higgs amplification is expected to occur in the terahertz, a frequency range that is of great current interest for fundamental science and technology

applications^{42,43}. The next section presents a calculation of Higgs amplification based on a semiclassical description of photons using Maxwell's equations. Our discussion is agnostic about the specific microscopic mechanism underlying light-induced superconductivity and, assuming that Higgs oscillations have been coherently excited, directly studies their effect on optical properties.

III. OPTICAL PROPERTIES OF A SUPERCONDUCTOR WITH AN EXCITED HIGGS MODE

The optical properties of a superconductor with an excited Higgs mode are understood as follows. Consider Maxwell's equations combined with the relation between the electrical current in the material and electric field:

$$\nabla \times \mathbf{B} - \frac{\epsilon}{c^2} \frac{\partial \mathbf{E}}{\partial t} = \mu_0 \mathbf{j}, \quad (2)$$

$$\nabla \times \mathbf{E} + \frac{\partial \mathbf{B}}{\partial t} = 0. \quad (3)$$

Here ϵ is the dielectric constant arising from bound charges and \mathbf{j} is the free current density. For $z > 0$, outside the superconductor, $\epsilon = \epsilon_{\text{out}}$ (in vacuum $\epsilon_{\text{out}} = 1$, but we allow for interfaces with other media) and we assume the current \mathbf{j} vanishes; for $z < 0$, $\epsilon = \epsilon_s$, and the current satisfies the London equation,

$$\mathbf{j} = \Lambda(t) \mathbf{v}_s. \quad (4)$$

Here, $\mathbf{v}_s = \frac{\hbar}{2e} \nabla \theta - \mathbf{A}$, where θ is the superconducting phase and \mathbf{A} is the vector potential. Note that $\partial_t \mathbf{v}_s = \mathbf{E}$. In an equilibrium superconductor, $\Lambda(t)$ reduces to the static value $\Lambda_s = \frac{e^2 n_s}{m}$, where n_s is the superfluid density. More generally, in a time-modulated superconductor, Eq. (4) describes accurately the total current induced by a vector potential \mathbf{A} in the limit where \mathbf{A} and Λ vary slowly compared to any microscopic frequencies such as the superconducting energy gap and the scattering rate $1/\tau$ for electrons in the normal state. We use it here under the assumption that it is at least a good starting approximation for the frequencies of interest to us.

In general, the value of Λ will depend on the value of the superconducting energy gap. (Although the special case of an ideal clean superconductor at $T = 0$ is an exception to this rule, we expect that the gap dependence will be manifest in the systems of interest to us, due to polaronic effects and coupling to impurities.⁴⁴) Since the Higgs mode represents a modulation in the energy gap, we expect it to induce a similar modulation in Λ . Consequently, we may write

$$\Lambda(t) = \Lambda_s + \Lambda_m e^{-i\omega_H t} + \Lambda_m^* e^{i\omega_H t} \quad (5)$$

where Λ_m describes the amplitude of the modulation, and ω_H is the Higgs mode frequency. For a BCS superconductor, $\omega_H = 2\Delta$, where Δ is the quasiparticle gap²².

Different frequencies mix due to the time dependence in Λ : incident light with frequency ω_1 will produce outgoing light with frequencies ω_1 and $\omega_2 = \omega_H - \omega_1$, see Fig. 1(c). Mixing of the Higgs modulation and the signal beam is also expected to induce light at the frequency $\omega_3 = \omega_1 + \omega_H$. We note, however, that the ω_3 frequency lies well above the quasiparticle threshold 2Δ , and we expect that this channel of mode mixing will be suppressed relative to the channel at ω_2 . This can be understood by observing that at such high frequencies the current should be carried primarily by quasiparticles, rather than supercurrents, and one might expect the quasiparticle current to be less sensitive than the supercurrent to modulations of the superconducting amplitude. In the remainder of this paper, for the sake of simplicity, we assume that excitation of the ω_3 mode is negligible, and we omit it entirely from our considerations. Our results should be qualitatively applicable, however, as long as excitation of the ω_3 mode is substantially weaker than that of the ω_2 mode.

Prior to solving the reflection problem, it is useful to first consider the evanescent wave solutions inside the superconductor. To simplify our discussion, we assume here that Λ_m is spatially uniform inside the superconductor. Non-uniformities in Λ_m due to the short penetration depth of the exciting radiation will be taken into account in the processing of the experimental data, as detailed in Appendix A. For the case of uniform Λ_m , the evanescent solutions are characterized by the spacetime dependence (\mathbf{V} stands for \mathbf{j} , \mathbf{v}_s , \mathbf{E} , or \mathbf{B}),

$$\mathbf{V} = (\mathbf{V}_1 e^{-i\omega_1 t} + \mathbf{V}_2^* e^{i\omega_2 t}) e^{\kappa z} + \text{c.c.} \quad (6)$$

Note that the same spatial dependence appears for ω_1 and $-\omega_2$ terms, since they mix with each other homogeneously in space. This should be contrasted with the static case, where each frequency mode decays with its own κ . Substituting Eq. (6) into Eq. (4) and collecting terms with frequencies ω_1 and $-\omega_2$ yields,

$$\mathbf{j}_1 = \Lambda_s \mathbf{v}_{s,1} + \Lambda_m \mathbf{v}_{s,2}^* = \Lambda_s \frac{\mathbf{E}_1}{-i\omega_1} + \Lambda_m \frac{\mathbf{E}_2^*}{i\omega_2}, \quad (7)$$

$$\mathbf{j}_2^* = \Lambda_s \mathbf{v}_{s,2}^* + \Lambda_m^* \mathbf{v}_{s,1} = \Lambda_s \frac{\mathbf{E}_2^*}{i\omega_2} + \Lambda_m^* \frac{\mathbf{E}_1}{-i\omega_1}. \quad (8)$$

For linearly polarized light, $\mathbf{E}_\nu = E_\nu \hat{e}_x$, $\mathbf{B}_\nu = B_\nu \hat{e}_y$, and $\mathbf{j}_\nu = j_\nu \hat{e}_x$, where $\nu \in \{1, 2\}$. Then, Eq. (3) yields $B_\nu = \frac{\kappa}{i\omega_\nu} E_\nu$, and Eq. (2) becomes

$$\begin{pmatrix} \kappa^2 c^2 + \omega_1^2 \epsilon_1 & \Upsilon \omega_1 / \omega_2 \\ \Upsilon^* \omega_2 / \omega_1 & \kappa^2 c^2 + \omega_2^2 \epsilon_2 \end{pmatrix} \begin{pmatrix} E_1 \\ E_2^* \end{pmatrix} = 0. \quad (9)$$

Here, $\Upsilon \equiv \Lambda_m / \epsilon_0$, $\epsilon_1 \equiv \epsilon(\omega_1)$, and $\epsilon_2 \equiv \epsilon(-\omega_2)$, where $\epsilon(\omega) = \epsilon_s - \Lambda_s / (\epsilon_0 \omega (\omega + i0^+))$ is the dielectric function of the superconductor [Note that, by changing the form of $\epsilon(\omega)$, one can generalize the discussion, *e.g.*, to introduce dissipation]. The allowed values of κ are obtained by requiring the determinant of the above matrix to vanish,

$$\kappa_\pm^2 c^2 = -\frac{\omega_1^2 \epsilon_1 + \omega_2^2 \epsilon_2}{2} \pm \sqrt{\frac{(\omega_1^2 \epsilon_1 - \omega_2^2 \epsilon_2)^2}{4} + |\Upsilon|^2}, \quad (10)$$

and the fields inside the superconductor satisfy,

$$\frac{E_{1,\pm}^t}{B_{1,\pm}^t} = \frac{i\omega_1}{\kappa_{\pm}} \equiv \eta_{\pm} \quad (11)$$

$$\frac{E_{2,\pm}^{t*}}{B_{1,\pm}^t} = \frac{-i\omega_2 (\kappa_{\pm}^2 c^2 + \omega_1^2 \epsilon_1)}{\Upsilon \kappa_{\pm}} \equiv \phi_{\pm} \quad (12)$$

$$\frac{B_{2,\pm}^{t*}}{B_{1,\pm}^t} = \frac{(\kappa_{\pm}^2 c^2 + \omega_1^2 \epsilon_1)}{\Upsilon} \equiv \gamma_{\pm} \quad (13)$$

where the superscript t indicates that these act as transmitted fields in the reflection problem.

Next, we consider a normally-incident signal beam of frequency ω_1 , and reflected beams at frequencies ω_1 and ω_2 , with

$$\mathbf{E}_1^i, \mathbf{B}_1^i \propto e^{-i\omega_1(t+z\sqrt{\epsilon_{\text{out}}}/c)}, \quad (14)$$

$$\mathbf{E}_\nu^r, \mathbf{B}_\nu^r \propto e^{-i\omega_\nu(t-z\sqrt{\epsilon_{\text{out}}}/c)}. \quad (15)$$

where $\nu \in \{1, 2\}$. The fields are linearly polarized as before, $\mathbf{E}_\nu = E_\nu \hat{e}_x$, $\mathbf{B}_\nu = B_\nu \hat{e}_y$, and Maxwell's equations constrain them to satisfy $E_1^i = -(c/\sqrt{\epsilon_{\text{out}}})B_1^i$ and $E_\nu^r = (c/\sqrt{\epsilon_{\text{out}}})B_\nu^r$. Within the superconductor, the transmitted fields are superpositions of two evanescent waves of the form (6) with $\kappa = \kappa_{\pm}$, whose amplitudes are fixed by boundary conditions imposed independently on each frequency:

$$B_1^i + B_1^r = B_{1,+}^t + B_{1,-}^t \quad (16)$$

$$E_1^i + E_1^r = E_{1,+}^t + E_{1,-}^t \quad (17)$$

$$B_2^{r*} = B_{2,+}^{t*} + B_{2,-}^{t*} \quad (18)$$

$$E_2^{r*} = E_{2,+}^{t*} + E_{2,-}^{t*} \quad (19)$$

Combining these with Eqs. (11), (12), and (13) yields

$$r \equiv \frac{B_1^r}{B_1^i} = \frac{(1 + \zeta) + \sqrt{\epsilon_{\text{out}}}(\eta_+ + \zeta\eta_-)}{(1 + \zeta) - \sqrt{\epsilon_{\text{out}}}(\eta_+ + \zeta\eta_-)}, \quad (20)$$

$$r_{12} \equiv \frac{B_2^{r*}}{B_1^i} = \frac{2(\gamma_+ + \zeta\gamma_-)}{(1 + \zeta) - \sqrt{\epsilon_{\text{out}}}(\eta_+ + \zeta\eta_-)}, \quad (21)$$

where

$$\zeta = -\frac{\gamma_+ - \sqrt{\epsilon_{\text{out}}}\phi_+}{\gamma_- - \sqrt{\epsilon_{\text{out}}}\phi_-}. \quad (22)$$

Eqs. (20) and (21) are the main theoretical results of this paper: r is the reflection amplitude of the signal beam, whereas r_{12} is the amplitude of the emitted idler mode at the down-converted frequency $\omega_2 = \omega_H - \omega_1$, normalized by the amplitude of the incident signal beam.

Figure 2 shows $R = |r|^2$ and $R_{12} = |r_{12}|^2$ as a function of ω_1 , in the case $\omega_H < \omega_{ps}$, where $\omega_{ps} = \sqrt{\Lambda_s/(\epsilon_0\epsilon_s)}$ is the superconducting plasma frequency of the material. Note that, in the absence of dissipation, there is amplification $R > 1$ over the entire range $0 < \omega_1 < \omega_H$, and the maximum amplification occurs at $\omega_1 = \omega_H/2$. One can study the effect of dissipation by writing $\epsilon(\omega) =$

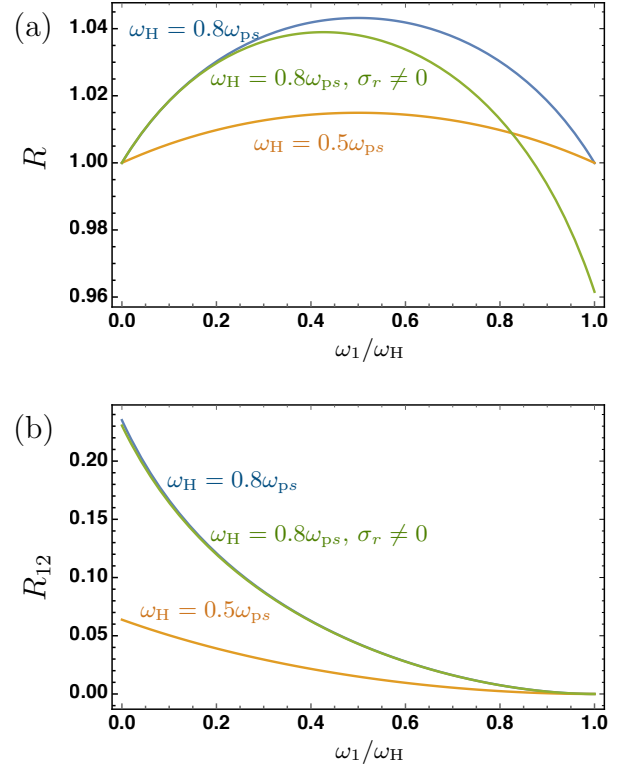


FIG. 2: (a) Reflection coefficient R and (b) downconversion intensity R_{12} as a function of the signal frequency ω_1 . We assume $\epsilon_s = 5$, $\epsilon_{\text{out}} = 5.62$ (corresponding to diamond), and $\Lambda_m = 0.4\Lambda_s$. Two different values of the Higgs frequency were taken, $\omega_H = 0.5\omega_{ps}$ and $\omega_H = 0.8\omega_{ps}$, where $\omega_{ps} = \sqrt{\Lambda_s/(\epsilon_0\epsilon_s)}$ is the superconducting plasma frequency. The green curves, corresponding to $\omega_H = 0.8\omega_{ps}$, illustrate the effects of dissipation, taken into account by assuming $\epsilon(\omega) = \epsilon_s - \sigma(\omega)/(i\epsilon_0\omega)$ with $\sigma(\omega) = \sigma_r + i\Lambda_s/(\omega + i0^+)$, where σ_r is a real constant; the blue and orange curves include no dissipation, $\sigma_r = 0$. Results are for the model in which Λ_m is uniform in space.

$\epsilon_s - \sigma(\omega)/(i\epsilon_0\omega)$ in Eqs. (20) and (21) and adding a real part to the conductivity function $\sigma(\omega)$. This suppresses the reflectivity and also reduces the frequency ω_1 at which the maximum occurs, as shown in Fig. 2(a).

Note that the net amplification in Fig. 2 is small, of the order of a few percent. In order to understand this, focus on $\omega_1 = \omega_2 = \omega_H/2$, where the maximum is obtained, with value

$$R_{\text{max}} = 1 + \frac{\epsilon_{\text{out}} \omega_H^2 (D_+ - D_-)^2}{[\epsilon_{\text{out}} \omega_H^2 + D_+ D_-]^2}, \quad (23)$$

where $D_{\pm} = \sqrt{4(\Lambda_s \pm |\Lambda_m|)/\epsilon_0 - \epsilon_s \omega_H^2}$. For $\omega_H^2 \ll \Lambda_s$ and $\Lambda_m \ll \Lambda_s$, this can be expanded to obtain

$$R_{\text{max}} = 1 + \frac{|\Lambda_m|^2 \epsilon_{\text{out}} \omega_H^2}{\Lambda_s^2 4 \epsilon_s \omega_{ps}^2}. \quad (24)$$

The factor $|\Lambda_m|^2/\Lambda_s^2$ expresses the fact that the amplification is proportional to the intensity of the modulation.

The factor $\epsilon_{\text{out}}\omega_{\text{H}}^2/(4\epsilon_{\text{s}}\omega_{\text{ps}}^2)$ is the square of the London penetration depth divided by the wavelength of the incident light; it expresses the fact that amplification is weak if the light cannot probe deeply into the superconductor. This suggests that, in order to enhance the amplification, one could consider instances in which the light can probe a larger region of the superconductor prior to being reflected. Two possible approaches to achieve this come to mind: First, by using incoming light with a shallow incidence angle to the sample, thus introducing geometrical factors which enhance the effect; second, by studying systems in which the Higgs frequency exceeds the plasma frequency. These possibilities will be discussed elsewhere⁴⁵. Note that, in a realistic superconductor, the penetration of light is controlled by the total plasma frequency ω_{p} , which receives contributions from all charge carriers, not just the superconducting ones. It is this total plasma frequency that presumably controls the strength of the Higgs amplification in Eq. (24).

In the next section, we will present experimental evidence for Higgs amplification in the superconductor K_3C_{60} . This is a natural candidate system for Higgs amplification. In this material, the low density of electrons (three per C_{60} molecule) and the weak hopping between C_{60} molecules conspire to yield an anomalously small plasma frequency $\omega_{\text{p}} = 72\text{meV}/\hbar$. Optical excitation at mid-infrared wavelengths has been shown to transform the high-temperature ($T \gg T_c$) metallic phase of K_3C_{60} into a transient non-equilibrium state with the same optical properties as the low temperature superconductor ($T < T_c$). The transient state, which is thought to be a photoinduced non-equilibrium superconductor, displays a saturated reflectivity ($R = 1$), a gap in the real part of the optical conductivity σ_1 and a divergent low-frequency imaginary conductivity σ_2 ⁷. In order to estimate the zero-temperature gap, 2Δ , at the light-induced state, we use the onset temperature for light-induced superconductivity, $T_{\text{light-induced}} \approx 100$ K, which yields $2\Delta \approx 30$ meV⁷. This gives an estimate for ω_{H} , which is expected to be reduced from this value at non-zero temperature (in the fit to our theory, we find ω_{H} is of the order of 24 meV/ \hbar , see Sec. V). Hence, K_3C_{60} combines a relatively large value of $\omega_{\text{H}}/\omega_{\text{p}}$, as necessary to enhance the reflectance in Eq. (24), together with the possibility for rapid quenches into the superconducting state by pump pulses, as needed to induce large Higgs oscillations. In particular, by modifying the type of quench protocol used, one may control the amplitude of Higgs oscillations.

The Higgs mode should be rather insensitive to the lack of long-range phase coherence, which is expected not to exceed a few coherence lengths in the photoinduced superconducting state. Hence, we expect the mechanism of Higgs amplification to occur in this case, despite the lack of global phase coherence.

IV. EXPERIMENTAL RESULTS

We follow the same protocol described in Ref. 7,8, to photo-induce the transient optical properties of a non-equilibrium superconductor in K_3C_{60} but using shorter and more intense pulses. To test the hypotheses discussed in the theory section above, we additionally analyzed conditions in which the quench was made slower with respect to the Higgs mode frequency of the photo-induced state. The pump pulse FWHM duration τ was tuned to different values between 100 fs and 1.8 ps. This range of pulse durations is interesting because it crosses a characteristic time scale $\tau^* = \hbar/(24\text{meV}) \sim 172$ fs, which corresponds to the period of the amplitude (Higgs) mode in the photo-induced superconductor. Note that in our experimental geometry the idler mode is not detected. In future studies, this mode could provide a measurement of the Higgs frequency and would allow for distinguishing Higgs amplification from other types of parametric amplification^{46,47}.

In the excitation regime explored in this experiment, when the pump pulse is significantly longer than τ^* , the transient state displays a reflection coefficient at the surface that is saturated at $R = 1$ for all frequencies below $\sim 10\text{meV}$. By reconstructing the complex optical conductivity with the same procedure used previously⁸, we extracted a gapped real optical conductivity σ_1 at all frequencies $\omega < 10$ meV and a divergent low-frequency imaginary conductivity σ_2 , indicative of a light-induced superconducting state. Our experiment reveals that as the pulse duration is made progressively shorter than τ^* , the transient state acquires a reflection coefficient that is larger than $R = 1$ immediately after the pump, indicative of optical amplification through the non-adiabatic creation of a superconducting state. The real part of the optical conductivity σ_1 is negative at all frequencies $\omega < 10$ meV while its imaginary part σ_2 remains divergent. Conceptually, the observed dependence on the pulse duration can be understood from the following consideration. Although the underlying mechanism of photo-induced superconductivity is still the subject of debate, we assume as a first approximation that the “effective” final state Hamiltonian experienced by the low-energy electrons depends only on the total pulse energy, and not its duration (later, we will show evidence that the shorter pulses actually do drive the superconductivity more strongly and induce a slightly larger superfluid density, although this is a weak effect). We furthermore assume that the superconducting state lasts longer than the probe sequence. Hence qualitatively we assume that by controlling the pump pulse duration we preserve the final effective Hamiltonian for electrons but change the rate at which the microscopic parameters are modified. In the case of a superconductor we expect that the Higgs-amplitude mode gets strongly excited when the interaction strength is modified on a time scale shorter than $\tau^* = \hbar/2\Delta$.

K_3C_{60} polycrystalline powders were excited at normal

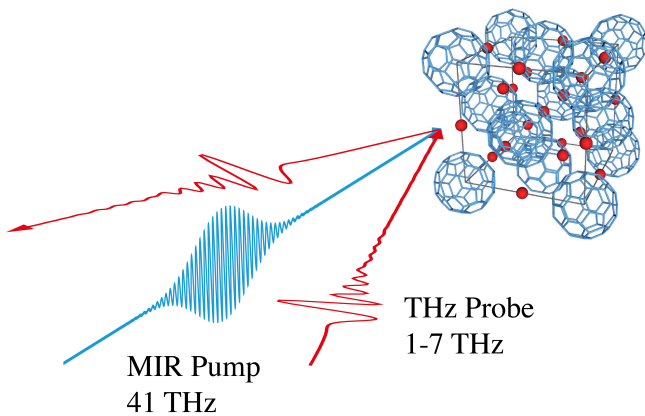


FIG. 3: Sketch of the experimental geometry. K_3C_{60} is excited with vertically polarized mid-infrared pulses. The THz probe pulses are polarized in the horizontal plane.

incidence with 170 meV linearly-polarized mid-infrared pulses. Their duration was tuned from 100 fs to 1.8 ps by chirping them through linear propagation in transparent and highly dispersive CaF_2 rods. For all pulse durations, the pulse energy and the number of incident photons were maintained constant. The transient low-frequency optical properties of photo-excited K_3C_{60} were retrieved as a function of pump-probe delay using transient terahertz time-domain spectroscopy using THz pulses with a bandwidth that ranged from 1 to 7 THz. These probe pulses were made to strike the sample at near normal incidence, with a 7° incidence angle (see Figure 3), and they were p -polarized, that is, with the electric field perpendicular to that of the MIR pump pulses. The measurement of the electric field reflected from the sample yielded a phase-resolved measurement of the reflection coefficient and through it the complex optical properties. The penetration depth of the mid-infrared pump (200nm) was shorter than that of the THz probe (600-900nm). To account for this, the data was analyzed as discussed in Appendix A in order to obtain the reflectivity corresponding to an effective semi-infinite and homogeneously pumped medium.

Figures 4(a) and 4(b) compare the transient optical properties of K_3C_{60} upon photoexcitation with intense mid-infrared pulses of 1.8 ps and 100fs duration, respectively. The red curves report the optical properties of the equilibrium metallic state, whilst the light-blue dots represent those of the transient state, measured at the peak of the response. For longer excitation pulses [1.8 ps, Fig. 4(a)] the transient optical properties resemble those of the equilibrium superconductor with a reflectivity saturated at $R = 1$, a gapped real conductivity ($\sigma_1 \approx 0$) and a divergent imaginary conductivity for all frequencies below ~ 10 meV. For $\tau = 100$ fs [Fig. 4(b)] we find that below ~ 10 meV, the reflectivity becomes larger than $R = 1$, reaching an average value in the gapped region of ~ 1.04 , with a maximum of ~ 1.06 . The extracted

real part of the optical conductivity is correspondingly negative, indicative of negative dissipation. These two observations suggest amplification of the incoming low frequency THz probe light. Importantly, the imaginary part of the optical conductivity maintained a $1/\omega$ behavior below ~ 10 meV, indicating the superconducting nature of the transient state.

The evolution of the optical properties for pump pulses either shorter or longer than τ^* can be captured by the average value of the reflectivity in the 5-8meV-frequency range and the superfluid density extracted by a $1/\omega$ fit to the imaginary part of the optical conductivity at low frequencies. Figure 5(a) and 5(b) show the evolution of these two quantities as a function of the duration of the excitation pulse (Fig. 5(b)). The average reflectivity in the gapped region decreases from ~ 1.04 to ~ 1 , as the pump pulse duration varies from 100 fs to 1.8 ps. The blue shaded area in the top panel highlights the regime where light amplification is observed. At the same time, the superfluid density of the photoinduced superconductor does not appear to strongly depend on the pulse duration of the excitation pulse.

V. COMPARISON OF THEORY AND EXPERIMENT

The experimental data does not give a direct measurement of the Higgs frequency – in the light-induced superconducting state, the gap measured in $\sigma_1(\omega)$ coincides with the lower edge of the mid-infrared absorption peak of K_3C_{60} , suggesting that the superconducting gap 2Δ is hidden under the spectral weight of this broad peak. However, there are two independent observations that give consistent estimates for ω_H . First, as argued earlier, the maximum of light amplification occurs slightly below $\omega_H/2$. The reflectivity measured with the shortest excitation pulse ($\tau = 100$ fs) shown in Fig. 4(a) would then suggest that ω_H is somewhat bigger than 20 meV/ \hbar . Second, as mentioned earlier, the onset temperature of the light-induced superconductivity corresponds to a gap $2\Delta(T = 0)$ of 30 meV/ \hbar for the zero-temperature transient superconductor. This gives an upper bound on ω_H , which tracks $2\Delta(T)$.

The measured optical conductivity $\sigma(\omega)$ has Higgs modulations built in. In order to make a comparison between theory and experiment, we need to model the optical conductivity of the static superconducting state, $\tilde{\sigma}$. We parametrize $\tilde{\sigma}$ as a sum of Drude and Lorentzian peaks:

$$\tilde{\sigma}(\omega) = \frac{\Lambda_s}{\gamma_D - i\omega} + \sum_{n=1}^3 \frac{B_n \omega}{i(\Omega_n^2 - \omega^2) + \gamma_n \omega} \quad (25)$$

The Lorentzians represent the broad mid-infrared absorption peak in K_3C_{60} ⁴⁸. For simplicity, we assume this peak to be unaffected by the onset of superconductivity, and fix the parameters B_n , Ω_n , and γ_n by fitting to the

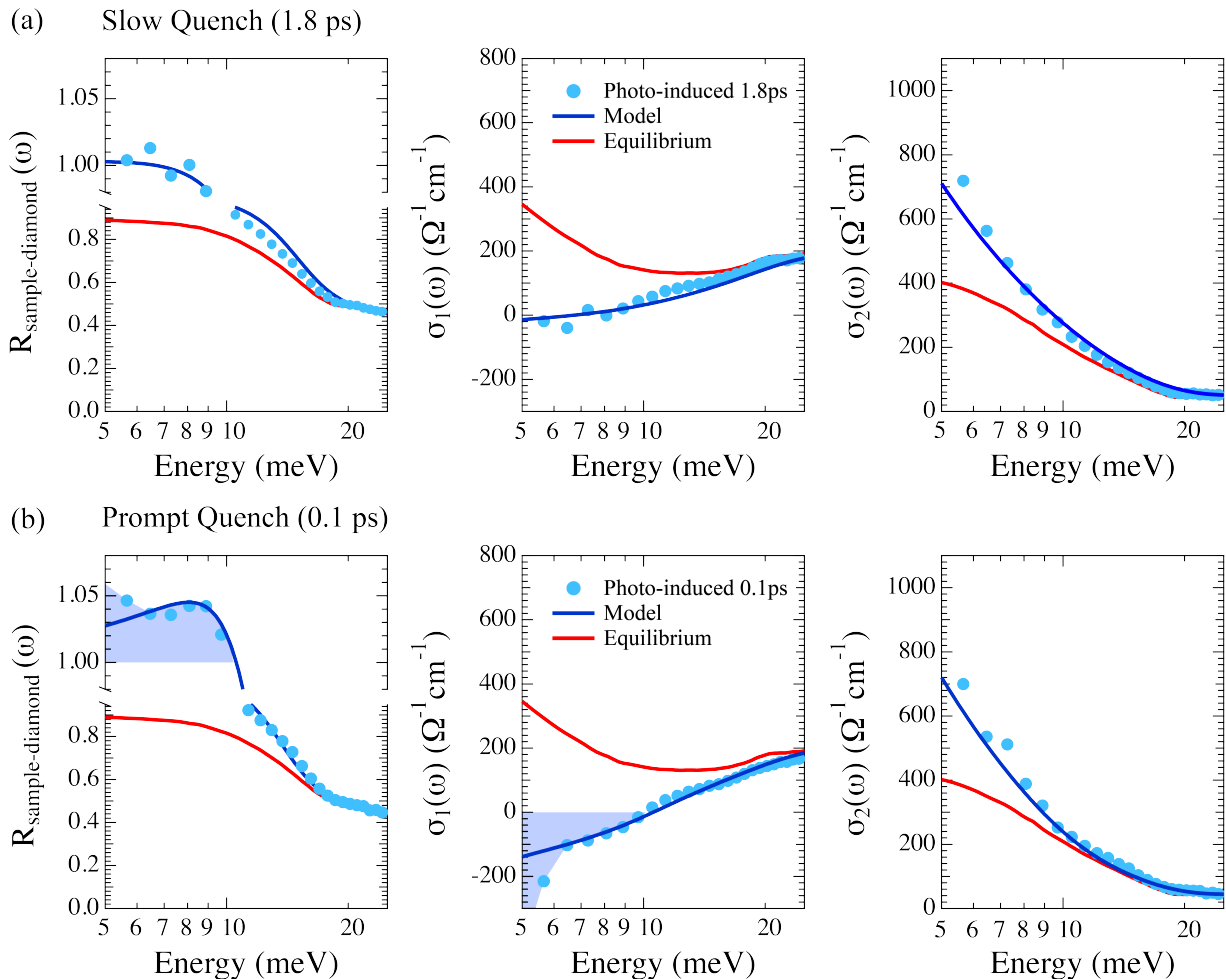


FIG. 4: (a) Reflectivity and complex optical conductivity (sample-diamond interface) of K_3C_{60} measured at equilibrium (red solid curves) and at the peak of the pump-probe response (light-blue dots) with pump pulse duration of 1800fs. For non-equilibrium systems we present inferred local quantities at the sample-diamond interface as discussed in Section V and Appendix A. (b) Same quantities, measured with pump pulse duration of 100fs. The shaded area highlights the frequency range where amplification is observed. All data were taken at $T=100\text{K}$ and at a fluence of $4.5\text{mJ}/\text{cm}^2$. The blue solid curves are the the optical conductivity and reflectivity calculated from the theoretical model taking into account Higgs modulations. The corresponding fit parameters are shown in Table I.

conductivity of the equilibrium normal state, as discussed in App. C. For the light-induced superconducting phase, we maintain the same values for the Lorentzian peaks, while for the Drude peak we replace $\gamma_{\text{D}} \rightarrow 0^+$ and allow Λ_{s} , which plays the role of the static superfluid density, to vary.

Given the static conductivity $\tilde{\sigma}$, we use the results of Section III to model the Higgs amplification phenomenon. We apply Eq. (20) to compute the complex reflection coefficient r at the signal frequency, in which we take $\epsilon(\omega) = \epsilon_{\text{s}} - \tilde{\sigma}(\omega)/(i\epsilon_0\omega)$. By inverting the Fresnel equation, r is then expressed as an effective optical conductivity $\sigma(\omega)$, see Sec. B, allowing us to make a comparison of the full complex response of the system.

We find that it is possible to describe the experimental data well by taking $\omega_{\text{H}} = 24 \text{ meV}/\hbar$. Then, for each value of τ , there are only two parameters we allow to

change, the superfluid density Λ_{s} and the amplitude of Higgs modulations, $\Lambda_{\text{m}}/\Lambda_{\text{s}}$. We emphasize that all other parameters in the model are determined in an unbiased manner by comparison with the equilibrium optical properties of the normal state. The blue solid curves in figure 4(a,b) shows the complex optical conductivity and the reflectivity of the superconductor with parameters as chosen in Table I. These results show good agreement with measurements, despite the limited number of fitting parameters used and the simplicity of the model, which does not take into account the full microscopic details of the system. In our fit, we find that the Higgs modulation amplitude increases with decreasing τ , in agreement with the expectation that shorter pulses give rise to more rapid quenches into the superconducting state, and therefore to larger Higgs oscillations. In addition, we find that Λ_{s} is slightly larger than its equilibrium value

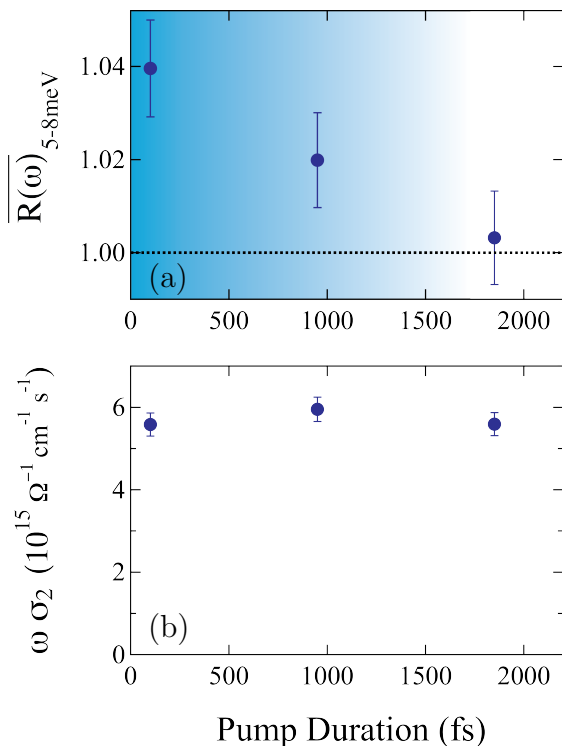


FIG. 5: (a) Inferred local transient reflectivity (sample-diamond interface), averaged between 5-8meV, as a function the pump pulse duration. The blue-shaded region indicates the range of pulse durations where amplification is observed. (b) $\omega \sigma_2(\omega \rightarrow 0) = \Lambda_s$, which is proportional to the transient superfluid density, extracted by a low frequency $1/\omega$ fit to $\sigma_2(\omega)$. All data were taken at $T=100\text{K}$ and a constant pump fluence of $4.5\text{mJ}/\text{cm}^2$.

in the normal state $\Lambda_{s,\text{eq}}$. This effect is larger for the shorter pulses. Even though the total pump pulse energy is maintained fixed, the shorter pulses have higher peak intensities, and can drive the superconductor more strongly since the pump drives the system nonlinearly. Note that, in order to preserve sum rules, this requires spectral weight to transfer from higher energies and may be an indication that the plasmonic peak must be modified in a complete microscopic description of the phenomenon.

τ (fs)	$\Lambda_s/\Lambda_{s,\text{eq}}$	Λ_m/Λ_s
1800	1.05	0.2
1000	1.11	0.37
100	1.17	0.47

TABLE I: Model parameters for different pump pulse widths.

The goal of our theoretical analysis was to provide the simplest physical picture of Higgs amplification. Therefore, we limited our discussion to the simplest case, in which the Higgs modulations were assumed to be monochromatic and spatially uniform. In practice, one may expect broadening of the Higgs excitation in fre-

quency, due to its finite lifetime, and in momentum, due to the non-equilibrium character of photoinduced superconductivity. This more comprehensive picture could be obtained by performing frequency and angle resolved measurements. However, these experiments would require more advanced instrumentation, including THz and IR free electron laser radiation. Importantly, this would allow for the separate measurement of both signal and idler amplification. This would provide direct access to the underlying non-linear dynamics of the photoinduced superconducting order parameter.

VI. OUTLOOK

We envision several potentially interesting applications of the Higgs amplification phenomenon. Of particular interest for quantum information is the possibility of generation of entangled photon pairs at THz frequencies, as expected from Eq. (1). Properties of the entangled photons may be controlled by tuning the intensity, duration, and angle of incidence of the pump beam.

The notions introduced above can be generalized to the non-linear dynamics of other kinds of non-equilibrium condensates, including charge and spin density waves, and excitonic condensates.

Systems with several competing orders should exhibit multiple finite energy collective modes, leading to an additional richness of the order parameter dynamics. The interaction between light and strongly excited collective modes opens a new frontier in the study of light-matter interaction in many-body quantum states.

Acknowledgments

We thank R. Averitt, I. Carusotto, J. Faist, M. Hatridge, A. Imamoglu, A. Georges, A. Millis, D. Pekker, and P. Zoller for illuminating discussions. We acknowledge financial support from the European Research Council under the European Union's Seventh Framework Programme (FP7/2007-2013)/ERC Grant Agreement No. 319286 (QMAC), the Deutsche Forschungsgemeinschaft via the excellence cluster 'The Hamburg Centre for Ultrafast Imaging Structure, Dynamics and Control of Matter at the Atomic Scale' and the priority program SFB925, the National Science Foundation (NSF), the Israel Science Foundation (grant 1803/18), the Harvard-MIT Center for Ultracold Atoms, DARPA DRINQS program (award D18AC00014), and the Vannavar Bush Faculty Fellowship. YW is supported by the Postdoctoral Fellowship of the Harvard-MPQ Center for Quantum Optics and the AFOSR-MURI Photonic Quantum Matter (award FA95501610323). DP is grateful for the hospitality of ITAMP at the Harvard-Smithsonian Center for Astrophysics, and of the Aspen Center for Physics, which is supported by NSF grant PHY-1607611.

Appendix A: Determining the optical conductivity of an equivalent homogenous medium

In the time-resolved experiments one measures the pump-induced difference in the complex reflected electric field $\Delta\tilde{E}_r(\omega)$. The “raw” complex reflection coefficient in the photo-excited state $\tilde{r}_{\text{pumped}}(\omega)$ can then be extracted by inverting the following equation:

$$\frac{\Delta\tilde{E}_r(\omega)}{\tilde{E}_r^0(\omega)} = \frac{\tilde{r}_{\text{pumped}}(\omega) - \tilde{r}_0(\omega)}{\tilde{r}_0(\omega)} \quad (\text{A1})$$

where $\tilde{r}_0(\omega)$ is the unperturbed complex reflection coefficient of K_3C_{60} known from broadband FTIR measurement and $\tilde{E}_r^0(\omega)$ is the reflected electric field in the unperturbed state. If the pump light penetrates in the sample several times more than the probe light, one can assume that the probe pulse samples a volume in the material that has been homogeneously transformed by the pump. In this case it is possible to directly extract the complex valued optical response functions by inverting the Fresnel equations.

The conditions assumed in the previous paragraph are not correct for the experiments presented here, because the penetration depth of the mid-infrared pump (220 nm) is at least three times shorter than that of the THz probe (600-900 nm). Nevertheless, it is instructive to see what results for the optical conductivity would be obtained if the assumption is made.

In the left panel of Fig. 6, we show raw data for the reflectivity, in equilibrium and after photoexcitation by pulses of three different lengths. In the second and third panels, we show the values of $\sigma_1(\omega)$ and $\sigma_2(\omega)$ that one would obtain from the observed reflectivities using the Fresnel equations, assuming optical conductivities independent of distance from the surface.

In contrast, the curves in Fig. 4 were obtained after taking account that the penetration depth of the probe radiation is longer than the that of the pump pulse, using the following approach. As the pump penetrates in the material, its intensity is reduced and it will induce progressively weaker changes in the refractive index of the sample. This is modeled by “slicing” the probed thickness of the material into thin layers where we assume that the pump-induced changes in the refractive index are proportional to the pump intensity in the layer, *i.e.* $\tilde{n}(\omega, z) = \tilde{n}_0(\omega) + \Delta\tilde{n}(\omega)e^{-\alpha z}$ where $n_0(\omega)$ is the unperturbed complex refractive index, α is the attenuation coefficient at the pump frequency, and z is the spatial coordinate along the sample thickness.

For each probe frequency ω_i , the complex reflection coefficient $\tilde{r}(\Delta\tilde{n})$ of such multilayer stack is calculated with a characteristic matrix approach⁴⁹ keeping $\Delta\tilde{n}$ as a free parameter. As equation (A1) relates directly the measured quantity $\Delta\tilde{E}_r(\omega)/\tilde{E}_r^0(\omega)$ to the changes in re-

flectivity we can extract $\Delta\tilde{n}$ by minimizing numerically:

$$\left| \frac{\Delta\tilde{E}_r(\omega_i)}{\tilde{E}_r^0(\omega_i)} - \frac{\tilde{r}(\omega_i, \Delta\tilde{n}) - \tilde{r}_0(\omega_i)}{\tilde{r}_0(\omega_i)} \right| \quad (\text{A2})$$

Note that $\Delta\tilde{n}(\omega)$ represents the pump-induced change in the refractive index at the surface, where the pump has not yet been attenuated by the absorption in the material. By taking $\tilde{n}(\omega) = \tilde{n}_0(\omega) + \Delta\tilde{n}(\omega)$ one can reconstruct the optical response functions of the material as if it had been homogeneously transformed by the pump.

The blue data points in Fig. 4 show the data processed in this manner to obtain the optical properties applicable to the region closest to the surface, where the excitation pulse is strongest. Specifically, panels in the second and third columns show the effective values of $\sigma_1(\omega)$ and $\sigma_2(\omega)$ deduced for this region, while the first column shows the reflectivity that would be expected if these values of the optical conductivity were to hold independent of depth. The blue solid curves show values obtained from the theoretical model with Higgs modulation. Comparing Figs. 4 and 6, we see that while the curves differ in detail, the enhanced optical response for the shortest pulse data, seen in both figures, tends to support our theoretical model. In particular, while we do not actually observe amplification in the raw reflected signal, our analysis suggests that amplification would have been observed if the pump pulse were able to penetrate more deeply into the sample.

Appendix B: Expressing the reflectivity in terms of a complex conductivity function

In the theory, we computed the complex reflection amplitude r , using Eq. (20). To convert this to a conductivity function, we used the Fresnel relation for the reflection amplitude at the interface between two media

$$r(\omega) = \frac{\sqrt{\epsilon_{\text{out}}} - i\sqrt{-\epsilon(\omega)}}{\sqrt{\epsilon_{\text{out}}} + i\sqrt{-\epsilon(\omega)}}. \quad (\text{B1})$$

For us, the first medium was diamond, which to a good approximation has a frequency-independent dielectric function $\sqrt{\epsilon_{\text{out}}} = 2.37$. This relation was inverted,

$$\epsilon(\omega) = \epsilon_{\text{out}} \left(\frac{1 - r(\omega)}{1 + r(\omega)} \right)^2, \quad (\text{B2})$$

in order to obtain the complex conductivity using $\sigma(\omega) = -i\epsilon_0\omega[\epsilon(\omega) - \epsilon_s]$.

Appendix C: Optical conductivity in the normal state

We model the optical conductivity $\tilde{\sigma}(\omega)$ of the equilibrium normal state as the sum of a Drude peak, representing the conduction band, and a sum of three Lorentzians,

Raw data: no correction for the inhomogeneous optical pump across the probed volume

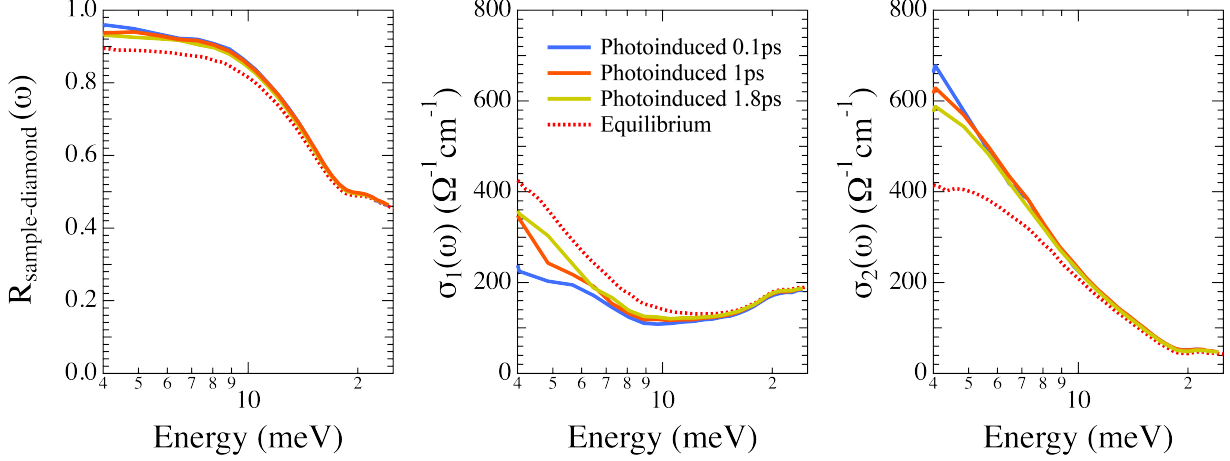


FIG. 6: The left panel shows raw data for the reflectivity (sample-diamond interface), in equilibrium and after photoexcitation by pulses of three different lengths. The second and third panels show the values of $\sigma_1(\omega)$ and $\sigma_2(\omega)$ that one would obtain from the observed reflectivity via the Fresnel equations, assuming optical conductivities independent of distance from the surface. Note that this neglects that the intensity of the pump pulse decays as a function of distance from the surface of the sample and the probe is sampling an inhomogeneously transformed volume.

representing a broad mid-infrared absorption peak⁴⁸.

$$\sigma_{\text{eq}}(\omega) = \frac{\Lambda_{\text{s,eq}}}{\gamma_{\text{D}} - i\omega} + \sum_{n=1}^3 \frac{B_n \omega}{i(\Omega_n^2 - \omega^2) + \gamma_n \omega} \quad (\text{C1})$$

A fit to the optical conductivity of the equilibrium normal state in the measured range $4\text{meV}/\hbar < \omega <$

$100\text{meV}/\hbar$ (see Figure 7) gives the following values: $\Lambda_{\text{s,eq}} = 3,470 \Omega^{-1}\text{cm}^{-1}\text{meV}/\hbar$, $\gamma_{\text{D}} = 3.56 \text{meV}/\hbar$, $B_1 = 18,300 \Omega^{-1}\text{cm}^{-1}\text{meV}/\hbar$, $\Omega_1 = 70.4 \text{meV}/\hbar$, $\gamma_1 = 86.6 \text{meV}/\hbar$, $B_2 = 4,600 \Omega^{-1}\text{cm}^{-1}\text{meV}/\hbar$, $\Omega_2 = 26.1 \text{meV}/\hbar$, $\gamma_2 = 34.0 \text{meV}/\hbar$, $B_3 = 2,400 \Omega^{-1}\text{cm}^{-1}\text{meV}/\hbar$, $\Omega_3 = 102.6 \text{meV}/\hbar$, $\gamma_3 = 35.0 \text{meV}/\hbar$.

- ¹ K. Nasu, *Photoinduced phase transitions* (World Scientific, 2004).
- ² M. Rini, A. Cavalleri, R. W. Schoenlein, R. López, L. C. Feldman, R. F. Haglund, L. A. Boatner, and T. E. Haynes, *Optics letters* **30**, 558 (2005).
- ³ V. R. Morrison, R. P. Chatelain, K. L. Tiwari, A. Hendaoui, A. Bruhács, M. Chaker, and B. J. Siwick, *Science* **346**, 445 (2014).
- ⁴ L. Stojchevska, I. Vaskivskiy, T. Mertelj, P. Kusar, D. Svetin, S. Brazovskii, and D. Mihailovic, *Science* **344**, 177 (2014).
- ⁵ J. Zhang, X. Tan, M. Liu, S. W. Teitelbaum, K. W. Post, F. Jin, K. A. Nelson, D. Basov, W. Wu, and R. D. Averitt, *Nature materials* **15**, 956 (2016).
- ⁶ D. Fausti, R. I. Tobey, N. Dean, S. Kaiser, A. Dienst, M. C. Hoffmann, S. Pyon, T. Takayama, H. Takagi, and A. Cavalleri, *Science* **331**, 189 (2011).
- ⁷ M. Mitrano, A. Cantaluppi, D. Nicoletti, S. Kaiser, A. Perucchi, S. Lupi, P. Di Pietro, D. Pontiroli, M. Riccò, S. R. Clark, et al., *Nature* **530**, 461 (2016).
- ⁸ A. Cantaluppi, M. Buzzi, G. Jotzu, D. Nicoletti, M. Mitrano, D. Pontiroli, M. Riccò, A. Perucchi, P. Di Pietro, and A. Cavalleri, *Nature Physics* **14**, 837 (2018), 1705.05939.
- ⁹ D. N. Basov, R. D. Averitt, and D. Hsieh, *Nature Materials*

- 16**, 1077 (2017).
- ¹⁰ T. Oka and S. Kitamura, *Annual Review of Condensed Matter Physics* **10**, 387 (2019), <https://doi.org/10.1146/annurev-conmatphys-031218-013423>, URL <https://doi.org/10.1146/annurev-conmatphys-031218-013423>.
- ¹¹ J. McIver, B. Schulte, F.-U. Stein, T. Matsuyama, G. Jotzu, G. Meier, and A. Cavalleri (2018).
- ¹² Y. H. Wang, H. Steinberg, P. Jarillo-Herrero, and N. Gedik, *Science* **342**, 453 (2013), ISSN 0036-8075.
- ¹³ W. Hu, S. Kaiser, D. Nicoletti, C. R. Hunt, I. Gierz, M. C. Hoffmann, M. Le Tacon, T. Loew, B. Keimer, and A. Cavalleri, *Nature Materials* **13**, 705 (2014), 1308.3204.
- ¹⁴ R. Mankowsky, A. Subedi, M. Först, S. O. Mariager, M. Chollet, H. T. Lemke, J. S. Robinson, J. M. Glownia, M. P. Minitti, A. Frano, et al., *Nature* **516**, 71 (2014), 1405.2266.
- ¹⁵ R. Matsunaga, Y. I. Hamada, K. Makise, Y. Uzawa, H. Terai, Z. Wang, and R. Shimano, *Physical review letters* **111**, 057002 (2013).
- ¹⁶ R. Matsunaga, N. Tsuji, H. Fujita, A. Sugioka, K. Makise, Y. Uzawa, H. Terai, Z. Wang, H. Aoki, and R. Shimano, *Science* **345**, 1145 (2014).
- ¹⁷ R. Matsunaga, N. Tsuji, K. Makise, H. Terai, H. Aoki, and R. Shimano, *Phys. Rev. B* **96**, 020505 (2017), 1703.02815.

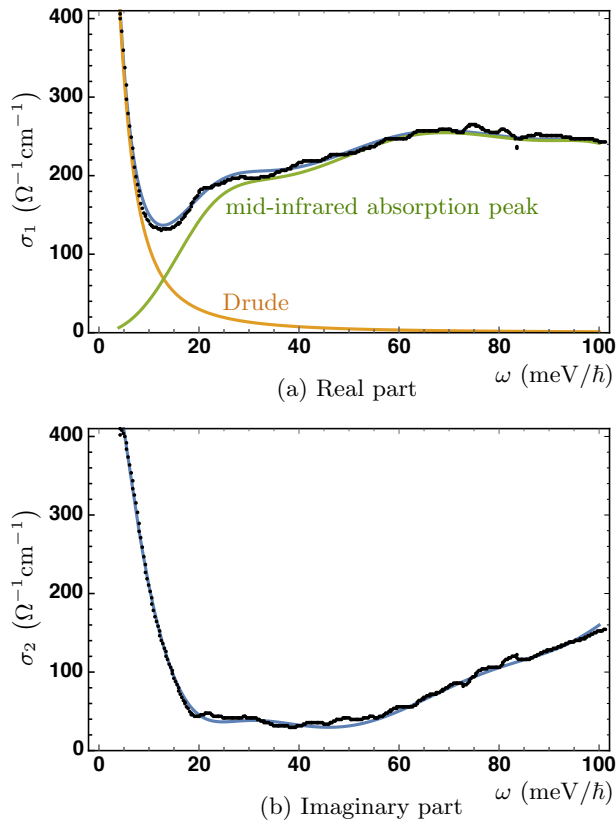


FIG. 7: Optical conductivity of the normal state at equilibrium. Black dots – measured conductivity. Blue curve – Fit to a sum of Drude and Lorentzian peaks, Eq. (C1). Orange and green curves – contributions to σ_1 arising from the Drude peak and Lorentzian peaks, respectively. The Lorentzian peaks represent a broad mid-infrared absorption peak, which we assume for simplicity not to be affected by the onset of superconductivity.

¹⁸ K. Katsumi, N. Tsuji, Y. I. Hamada, R. Matsunaga, J. Schneeloch, R. D. Zhong, G. D. Gu, H. Aoki, Y. Gallais, and R. Shimano, *Physical Review Letters* **120**, 117001 (2018), 1711.04923.

¹⁹ A. Dienst, E. Casandruc, D. Fausti, L. Zhang, M. Eckstein, M. Hoffmann, V. Khanna, N. Dean, M. Gensch, S. Winnerl, et al., *Nature Materials* **12**, 535 (2013).

²⁰ S. Rajasekaran, E. Casandruc, Y. Laplace, D. Nicoletti, G. D. Gu, S. R. Clark, D. Jaksch, and A. Cavalleri, *Nature Physics* **12**, 1012 (2016), 1511.08378.

²¹ R. Sooryakumar and M. Klein, *Physical Review Letters* **45**, 660 (1980).

²² P. Littlewood and C. Varma, *Physical Review B* **26**, 4883 (1982).

²³ C. Varma, *Journal of Low Temperature Physics* **126**, 901 (2002).

²⁴ D. Sherman, U. S. Pracht, B. Gorshunov, S. Poran, J. Jesudasan, M. Chand, P. Raychaudhuri, M. Swanson, N. Trivedi, A. Auerbach, et al., *Nature Physics* **11**, 188 (2015).

²⁵ C. Rüegg, B. Normand, M. Matsumoto, A. Furrer, D. F. McMorrow, K. W. Krämer, H. U. Güdel, S. N. Gvasaliya, H. Mutka, and M. Boehm, *Phys. Rev. Lett.*

100, 205701 (2008), URL <http://link.aps.org/doi/10.1103/PhysRevLett.100.205701>.

²⁶ Y. Ren, Z. Xu, and G. Lupke, *The Journal of Chemical Physics* **120**, 4755 (2004).

²⁷ J. P. Pouget, B. Hennion, C. Escribe-Filippini, and M. Sato, *Phys. Rev. B* **43**, 8421 (1991), URL <http://link.aps.org/doi/10.1103/PhysRevB.43.8421>.

²⁸ R. Yusupov, T. Mertelj, V. Kabanov, S. Brazovskii, P. Kusar, J. Chu, I. Fisher, and D. Mihailovic, *Nature Physics* (2010).

²⁹ M. Endres, T. Fukuhara, D. Pekker, M. Cheneau, P. Schauß, C. Gross, E. Demler, S. Kuhr, and I. Bloch, *Nature* **487**, 454 (2012).

³⁰ U. Bissbort, S. Götze, Y. Li, J. Heinze, J. S. Krauser, M. Weinberg, C. Becker, K. Sengstock, and W. Hofstetter, *Phys. Rev. Lett.* **106**, 205303 (2011).

³¹ S. Denny, S. Clark, Y. Laplace, A. Cavalleri, and D. Jaksch, *Phys. Rev. Lett.* **114**, 137001 (2015).

³² D. M. Kennes, E. Y. Wilner, D. R. Reichman, and A. J. Millis, *Nat. Phys.* **13**, 479 (2017).

³³ A. Nava, C. Giannetti, A. Georges, E. Tosatti, and M. Fabrizio, *Nat. Phys.* **14**, 154 (2018).

³⁴ M. Babadi, M. Knap, I. Martin, G. Refael, and E. Demler, *Phys. Rev. B* **96**, 014512 (2017).

³⁵ R. A. Barankov, L. S. Levitov, and B. Z. Spivak, *Phys. Rev. Lett.* **93**, 160401 (2004), URL <https://link.aps.org/doi/10.1103/PhysRevLett.93.160401>.

³⁶ E. A. Yuzbashyan, O. Tsypliyatyev, and B. L. Altshuler, *Phys. Rev. Lett.* **96**, 097005 (2006), URL <https://link.aps.org/doi/10.1103/PhysRevLett.96.097005>.

³⁷ R. A. Barankov and L. S. Levitov, *Phys. Rev. Lett.* **96**, 230403 (2006), URL <https://link.aps.org/doi/10.1103/PhysRevLett.96.230403>.

³⁸ P. Calabrese, F. H. L. Essler, and M. Fagotti, *Journal of Statistical Mechanics: Theory and Experiment* **2012**, P07016 (2012).

³⁹ A. A. Clerk, M. H. Devoret, S. M. Girvin, F. Marquardt, and R. J. Schoelkopf, *Reviews of Modern Physics* **82**, 1155 (2010).

⁴⁰ D. Podolsky, A. Auerbach, and D. P. Arovas, *Phys. Rev. B* **84**, 174522 (2011).

⁴¹ Z. Ou, *Physical Review A* **78**, 023819 (2008).

⁴² H. Y. Hwang, S. Fleischer, N. C. Brandt, B. G. Perkins Jr, M. Liu, K. Fan, A. Sternbach, X. Zhang, R. D. Averitt, and K. A. Nelson, *Journal of Modern Optics* **62**, 1447 (2015).

⁴³ M. Graf, G. Scalari, D. Hofstetter, J. Faist, H. Beere, E. Linfield, D. Ritchie, and G. Davies, *Applied Physics Letters* **84**, 475 (2004).

⁴⁴ D. C. Mattis and J. Bardeen, *Phys. Rev.* **111**, 412 (1958), URL <https://link.aps.org/doi/10.1103/PhysRev.111.412>.

⁴⁵ Y. Wang, D. Podolsky, and E. A. Demler (2019).

⁴⁶ A. Cartella, T. F. Nova, M. Fechner, R. Merlin, and A. Cavalleri, *Proceedings of the National Academy of Sciences* **115**, 12148 (2018), ISSN 0027-8424.

⁴⁷ H. Y. Liu, I. Gierz, J. C. Petersen, S. Kaiser, A. Simoncig, A. L. Cavalieri, C. Cacho, I. C. E. Turcu, E. Springate, F. Frassetto, et al., *Phys. Rev. B* **88**, 045104 (2013).

⁴⁸ M. J. Rice and H.-Y. Choi, *Phys. Rev. B* **45**, 10173 (1992), URL <https://link.aps.org/doi/10.1103/PhysRevB.45.10173>.

⁴⁹ M. Born and E. Wolf, *Principles of Optics* (Pergamon Press, 1970), 4th ed.